의학박사 학위논문

The Anticancer Effect of Artesunate-Induced Ferroptosis and Its Role for Overcoming Oxaliplatin Resistance in Pancreatic Cancer

췌장암에서 아르테수네이트 유도성 퍼롭토시스의 항암효과와 이를 통한 옥살리플라틴 내성의 극복

2023년 2월

서울대학교 대학원

의학과 내과학

최 진 호

A thesis of the Degree of Doctor of Philosophy

The Anticancer Effect of Artesunate-Induced Ferroptosis and Its Role for Overcoming Oxaliplatin Resistance in Pancreatic Cancer

February 2023

Graduate School of Medicine

Seoul National University

Internal Medicine

Jin Ho Choi

췌장암에서 아르테수네이트 유도성 퍼롭토시스의 항암 효과와 이를 통한 옥살리플라틴 내성의 극복

지도교수 김 용 태

이 논문을 의학박사 학위논문으로 제출함

2022년 10월

서울대학교 대학원

의학과

최 진 호

최진호 의 박사 학위논문을 인준함

2023년 1월

위 원 장 류 지 곤

부위원장 김 용 태

위 원 이 상 협

위 원 구 자 록

위 원 이 준 규

Abstract

Pancreatic cancer (PC) remained one of the worst prognostic cancers. Despite of extension of life expectancy with the combination of cytotoxic chemotherapy for patients with PC, resistance and non-responsiveness cause impediment of limited treatment efficacy. Overcoming these remains important clinical unmet needs. In this study, the effect of artesunate (ART) -induced ferroptosis on pancreatic cancer was evaluated by using PC cell lines and patient-derived pancreatic cancer organoids (PDPCOs). Four commercial PC cell lines, and 5 PDPCOs with various KRAS mutation and oxaliplatin (OXA) resistance were used in this study. Cell viability assay, migration and invasion assay, and spheres formation assay were conducted to measure the efficacy of ART for PC. PDPCOs with KRAS wild type did not show effective cell death by ART. PDPCOs with $KRAS^{G12V}$ mutation showed the most effective anti-cancer effect by ART, and ART showed a synergistic effect in PDPCOs with KRAS mutation regardless of the mutation subtype. Reactive oxygen species detection, lipid peroxidation assay, and labile iron pool assay were conducted to evaluate ferroptosis. Molecular pathways of action for ART-induced ferroptosis were evaluated by quantitative real-time PCR and western blotting. ART showed a significant anticancer effect with ferroptosis to PC cell lines and PDPCOs, rather than apoptosis. ART effectively induced ferroptosis even in OXA-resistant PDPCOs, and the synergistic effect of ART with OXA was shown accompanying by the enhanced level of ferroptosis. ART effectively induced ferroptosis in PC to induce an elevated level of intracellular iron

level by overexpression of the iron-import metabolic pathway. The promising anticancer effect and potential to overcome OXA resistance in PC of ART-induced ferroptosis by dysregulation of iron homeostasis were confirmed in this study. According to the comprehensive analytic results from differential expressed genes analysis, gene set enrichment analysis, pathway analysis, and protein-protein interaction network analysis, upregulation of ceruloplasmin was suspected as a key biomarker for the prediction of ART unresponsiveness. Further clinical trials in human subjects to overcome OXA resistance in PC using ART are needed in near future.

Keyword : Pancreatic cancer; Artesunate; Ferroptosis; Organoids; Drug resistance

Student Number : 2020-30048

Table of Contents

LIST OF TABLES AND FIGURES

Figure 4. Result of artesunate, oxaliplatin, and their combinatorial treatment for patients-derived pancreatic cancer organoids. (A) Result of cell viability assay for artesunate, oxaliplatin, and their combinatorial treatment for eight patients-derived pancreatic cancer organoids (B) Representative confocal images of patients-derived pancreatic cancer organoids

Figure 5. Artesunate-induced ferroptosis is a key mechanism of anticancer effect for pancreatic cancer. (A) cytotoxic effect of ART and reversal with ferroptosis inhibitors (B) Lipid peroxidation with C11-BODIPY fluorescence assay for ART-induced lipid peroxidation and its reversal with Fer-1 (C) Lipid peroxidation assay with measurement of malondialdehyde concentration and its reversal with ferroptosis inhibitors (D) DCF-DA fluorescence assay for ART-induced ferroptosis and its reversal with Fer-1 (E) Cytotoxic effect of ART and no reverse effect with an apoptosis inhibitor

Figure 6. Role of ferroptosis in the combinatorial effect of artesunate and oxaliplatin. (A) Result of lipid peroxidation assay (B) Result of labile iron pool assay (C) Result of detection of ROS level (D) Result of mitochondrial ROS assay

Figure 7. Exploration of artesunate-induced ferroptosis. (A) Result of iron metabolism-related RNA expression (B) Result of a western blot for iron metabolism pathway

Figure 8. Result of differential expressed gene analysis and gene set enrichment analysis according to response for artesunate. (A) The number of differentially

expressed genes between ART responder and ART non-responder (B) Heatmap of differentially expressed genes between ART responder and ART non-responder (C) Volcano plot of differentially expressed genes between ART responder and ART non-responder (D) Identification of core differentially expressed genes between responders and non-responders. Consideration of top 50 genes from the comparison of enrichment analysis by KEGG pathway and functional protein association networks analysis with iron homeostasis related genes by Sting-DB. The bottom panel shows the result of identified genetic alterations in the non-responders. (E) Ferroptosis-related pathway analysis with the KEGG database

Figure 9. The schematic diagram for the mechanism of artesunate-induced ferroptosis

LIST OF ABBREVIATIONS

ART: artesunate

Ceruloplasmin: CP

Differentially expressed genes: DEGs

GAPDH: glyceraldehyde 3-phosphate dehydrogenase

IC_{50}: the half maximal inhibitory concentration

Kyoto Encyclopedia of Genes and Genomes: KEGG

KRAS: Kirsten rat sarcoma viral oncogene homolog

LIP: labile iron pool

OXA: oxaliplatin

PC: pancreatic cancer

PDPCO: patient-derived pancreatic cancer organoid

ROS: reactive oxygen species

TFRC: transferrin receptor 1

WT: wild type

Chapter 1. Introduction

Pancreatic cancer (PC) remained one of the worst prognostic cancers, with an estimated overall five-year survival rate under 10%, and it is expected to be the second-most primary cause of death by 2030.[1,2] Despite advances in treatments leading to better clinical outcomes, improving prognosis of PC is confronted with great difficulty compared to other cancers. Combination therapy of cytotoxic anticancer drugs has contributed a lot to the extension of life expectancy of patients with PC, but resistance and non-responsiveness cause impediments of limited treatment efficacy.[3,4] KRAS mutations are identified in 90% of PC that is known to be induced the resistance and evasion of the cytotoxic effect of anticancer drugs.[5,6] There remains the most important unmet need for anticancer drugs with de novo mechanisms that can overcome the resistance of chemotherapy in PC.

Recently, several drugs were revealed to trigger regulated non-apoptotic cell death, which is different from the traditional anticancer mechanisms that induce apoptotic cell death.[7] Ferroptosis, a representative mechanism of non-apoptotic cell death, was suggested to be a new promising way to kill cancer cells resistant to chemotherapy.[8,9] Cancer cells exhibit an increased iron demand compared with normal cells, which can make cancer cells more vulnerable to iron-catalyzed cell death mechanism.[10] Ferroptosis inducers were suggested to overcome the resistance of cytotoxic anticancer drugs through combination with existing cytotoxic anticancer drugs with promising preclinical studies including renal cell carcinoma, colorectal cancer, head and neck cancer, gastric cancer, lung cancer, glioblastoma, and breast cancer.[11-17] Ferroptosis was induced with several known drugs and substances

including erastin, sorafenib, sulfasalazine, glutamate, FIN56, Ras-selective lethal compound 3, HMG-CoA reductases, and artesunate (ART).[18]

ART, which is used as a treatment for malaria, is known to induce ferroptosis, and showed promising cytotoxic effects for several types of cancers.[19] There was a study of the anticancer effect of ART in 2D-cultured PC cell lines, which reported the lethal cytotoxic effect of ART for PC with constitutive-activated KRAS, and ART did not affect normal human pancreatic ductal epithelial cells.[20] Since ART-induced ferroptosis can be a breakthrough that overcomes the resistance to apoptosis of PC, it is important to validate this more advanced manner. In this study, we tried to evaluate the effect of ART on PC, using PC cell lines and patient-derived pancreatic cancer organoids (PDPCOs) which were established from endoscopic ultrasound-guided fine needle biopsy in our institution.[21] Cancer organoids were proposed that potentially fill the gap between simple cancer cell lines and complicated, but physiologically relevant xenografts.[22-24] Further, preclinical studies with 2D-cultured PC cell lines were conducted to evaluate the efficacy of ART in various conditions including KRAS mutation, resistance to oxaliplatin, and combinatorial treatment and PDPCOs, and to find the role and underlying mechanism of ART-induced ferroptosis.

Chapter 2. Materials and Methods

2.1. Cell cultures and chemicals

Panc-1, MiaPaCa-2, AsPC-1, and BxPC-3 cell lines were purchased from the American Type Culture Collection (ATCC; Manassas, VA, USA) and the Korea Cell Line Bank (KCLB, Korea). The AsPC-1 cells were cultured in RPMI (Gibco, CA, USA) containing 10% fetal bovine serum (FBS; Invitrogen, Carlsbad, CA, USA) and 1% penicillin/streptomycin (PS; Gibco). Panc-1, MiaPaCa-2, and BxPC-3 cells were cultured in DMEM (Gibco) containing 10% FBS and 1% PS. Cells were maintained at 37 °C in a humidified atmosphere of 95% air and 5% CO2 and periodically screened for Mycoplasma contamination. The characteristics of PC cell lines used in this study were shown in **Table 1**.

ART was purchased from Tokyo Chemical Company (TCI; Shanghai, China). OXA was purchased from Sigma-Aldrich (St. Louis, Mom USA). Ferrostatin-1 (Fer-1), Trolox, and Deferoxamine (DFO) were purchased from Selleckchem (Houston, TX, USA). Carbobenzoxy-valyl-alanyl-aspartyl-[O-methyl]-fluoro-methyl ketone (zVAD.fmk) was purchased from R&D Systems, Inc. (Minneapolis, MN, USA).

2.2. PDPCO culture

The collection of PC patient data and tissue for an organoid generation was performed by the guidelines under the approval of the Institutional Review Board of

Seoul National University Hospital (IRB no. 1102-098-357; 1712-056-905; 2003-189-1112, Seoul, Korea). Patient-derived cell lines and PDPCOs were established from core biopsy tissue from endoscopic ultrasound-guided fine needle biopsy by one experienced endoscopist. PDPCOs were provided by Korean Cell Line Bank (SNU-3947-TO, SNU-4206-TO, SNU-4305-TO, SNU-4340-TO, and SNU-4354-TO). All organoids were grown in a medium consisting of Wnt3a/R-spondin1/Noggin-conditioned medium (50% vol/vol), containing 1×B27 supplement (Life Technologies, Carlsbad, CA, USA), 0.5 mM N-acetyl-L-cysteine (Sigma-Aldrich), 10 mM nicotinamide (Sigma-Aldrich), 50 ng/mL human epithelial growth factor (EGF; PeproTech Inc., Cranbury, NJ, USA), 500 nM A83-01, 100 ng/mL human fibroblast growth factor 10 (FGF10; PeproTech), and 10 nM gastrin (R&D Systems, Inc.; Minneapolis, MN, USA) in Advanced DMEM/F12 (Life Technologies) medium. For passaging, organoids were collected, washed, and disrupted either by mechanical shearing or digestion with TrypLE Express (Life Technologies), and organoid fragments were replated in fresh Matrigel (Corning, NY, USA) or BME type 2 (Trevigen, Gaithersburg, MD, USA). The detailed procedure and methods for the establishment and maintenance of patient-derived cell lines and PDPCOs were described in the previous study.[21] The characteristics of PDPCOs used in this study were shown in **Table 1**.

2.3. Cell viability assay

Cells were plated in triplicate (3,000 cells/well) and incubated in a medium containing 10% FBS. For cytotoxicity assay, after 24 hours, the complete medium

was replaced with the test medium containing the vehicle control and various doses (0 ~ 100 μM) of drugs (ART or OXA, respectively) at 48 hours at 37°C. For inhibitor assay, cells were preincubated with Fer-1 (1 μM, 2 hours), Trolox (40 μM, 6 hours), DFO (AsPC-1 and Panc-1, 1 μM, 6 hours; MiaPaCa-2, 6 μM, 6 hours), and z-VAD.fmk (10 μM, 2 hours) before treatment with ART. For drug combination experiments, cells were treated with the OXA (AsPC-1 and Panc-1, 100 μM; MiaPaCa-2, 25 μM) and ART (AsPC-1, 10 μM; Panc-1 and MiaPaCa-2, 20 μM) for 24 hours. Cell viability was assessed by measuring intracellular levels of ATP using the Cell Titer-Glo luminescent cell viability assay kit (Promega, Madison, USA).

Drug cytotoxicity in 3D spheroid assembly cultures was performed as previously described.[25] Briefly, cells (1,000 cells/well) were seeded in U-bottom-shaped 96-well plates (Corning) and grown into spheroids for 2 days, followed by drug treatment at the above concentrations. For cytotoxicity experiments in the PDPCO model, organoids dissociated into single cells, and 600 viable cells were seeded per well in 50 μL (50% Matrigel or BME: 50% human complete organoid media). After 72 hours of ART and/or OXA treatment, 3D cell viability was assessed by measuring the intracellular levels of ATP using the Cell Titer-Glo 3D luminescent cell viability assay kit (Promega). Luminescence was measured on a Luminometer (Glomax®Explore Multimode Microplate Reader, Promega, USA). Data were normalized to the control group (vehicle), and the half maximal inhibitory concentration (IC_{50}) value calculations were made using Hill's equation for GraphPad Prism software 8 (GraphPad Inc., San Diego, CA, USA).

2.4. Migration and invasion assay

Transwell migration assays were performed in a chamber system, and 2–5 × 10^5 cells suspended in 100 μL DMEM without serum were added to the upper chamber of a 6.5 mm (8 μm pore size) 24-well transwell (Corning).[26] DMEM with 10% FBS was placed into the bottom wells. Invasion assays were the same chamber system using Matrigel (corning) coating. Then, the upper chamber was washed with PBS, fixed with 4% paraformaldehyde for 10 min, and stained with crystal violet. Images were acquired using an inverted microscope (Nikon, Tokyo, Japan) and calculated staining cells.

2.5. Spheres formation assay

Cells were collected and washed to remove serum, then suspended in serum-free DMEM/F12 supplemented with 20 ng/ml human EGF (PeproTech), 20 ng/ml human recombinant basic fibroblast growth factor (bFGF, PeproTech), and 1XB27 supplement (life technology). The cells were subsequently cultured in ultra-low attachment 96-well plates (Corning) at a density of 2,000 cells/well. Sphere-forming efficacy was calculated by counting the number of spheroids with a size of 100 μm or more.[27]

2.6. ROS detection

The intracellular ROS and mitochondrial-generated superoxide were

determined by H2DCFDA (Invitrogen) and MitoSOX red (Invitrogen) using flow cytometry analysis because some ferroptosis inducers lead to cell death step by step as mitochondrial hyperpolarization, mitochondrial ROS generation, mitochondrial dysfunction, and ferroptotic execution.[28,29] Cells were incubated with 10 μM DCFH-DA probe (15 min) and 2.5 μM MitoSox red (30 min) at 37°C. The cell suspension was immediately analyzed on a BD FACSCaliber (BD Biosciences, Franklin Lakes, NJ, USA). All data were processed using the FlowJo™ 10 software.

2.7. Lipid peroxidation assay

A lipid peroxidation assay was conducted to evaluate for excessive phospholipid peroxidative level, which distinguishes ferroptosis from other cell death mechanisms.[30] The relative malondialdehyde (MDA) concentration in cell lysates was assessed using a Lipid Peroxidation Assay Kit (Abcam, Cambridge, MA, USA) according to the manufacturer's instructions. Briefly, the MDA in the sample reacted with thiobarbituric acid (TBA) to generate an MDA-TBA adduct. The MDA-TBA adduct was quantified colorimetrically (OD = 532 nm) or fluorometrically (Ex/Em = 532/553 nm).

The relative lipid ROS level in cells was assessed using C11-BODIPY dye (Thermo Fisher Scientific). Cells were treated with 5 μM C11-BODIPY for 30 min, harvested, and washed twice with PBS. Oxidation of the polyunsaturated butadienyl portion of the dye results in a shift of the fluorescence emission peak from ~590 to ~510 nm, which was detected by flow cytometry (BD Bioscience). The relative lipid peroxidation level was calculated using the mean fluorescence intensity (MFI).

2.8. Labile iron pool (LIP) assay

Total cellular iron was measured using the Calcein-AM assay Kit (Thermo Fisher). In brief, cells were washed with PBS and subsequently stained with Calcein-AM (1 μM) in PBS for 15 min at 37°C. Calcein-AM was removed from the cells, and the cell suspension was immediately analyzed on a BD FACSCaliber (BD Biosciences, Franklin Lakes, NJ, USA).[31] Data were processed using the FlowJo™ 10 software.

2.9. Evaluation of the combination effect of drugs

To analyze drug combination profiling data, we calculated synergy scores with SynergyFinder (version 2.0) that implemented four reference synergy models (highest single agent, Bliss, Loewe, and zero interaction potency) and their extensions to calculate synergy scores for higher-order combination data.[32] According to the synergy score, the interaction between two drugs is likely to be antagonistic (less than -10), additive (from -10 to 10), and synergistic (larger than 10). This platform is freely available for use on the website: [https://synergyfinder.fimm.fi/synergy/synfin_docs/].

2.10. Quantitative real-time PCR (qPCR)

Total RNA was isolated from cells using the AccuPrep® Universal RNA Extraction Kit (Bioneer, Daejeon, Korea) according to the manufacturer's protocol. Genomic DNA was removed by DNase treatment using RNase-Free-DNase Set (Qiagen, Hilden, Germany). cDNA was synthesized using AccuPower® RocketScript Cycle RT PreMix (Bioneer). Data were normalized to the expression levels of glyceraldehyde 3-phosphate dehydrogenase (GAPDH) or β-actin. The following primer sequences (5'-3') were used: GPX4, (forward) GCCAGGGAGTAACGAAGAGAT, (reverse) TTGATGGCATTTCCCAGGATG; SLC7A11, (forward) ACAGGGATTGGCTTCGTCAT, (reverse) GGGCAGATTGCCAAGATCTCA; Transferrin, (forward) TGTTCCGGTCGGAAACCAAG, (reverse) TTTGGTTGCCACTTCCCCAT; Transferrin Receptor 1 (TFRC), (forward) GGACGCGCTAGTCTTCT, (reverse) CATCTACTTGCCGAGCCAGG. Data analysis was based on the relative quantitative method, and ΔCT value was used to determine the relative fold change in the expression.

2.11. Western blotting

Cells were collected and homogenized in RIPA lysis buffer (Thermo Fisher) on ice. Subsequently, the cell lysates were centrifuged at 4 °C to separate the proteins. Proteins were quantified using a Bicinchoninic Acid Protein Assay kit (Thermo Fisher). Western blotting was performed using anti-SLC7A11, SLC3A2, SLC11A2 (DMT1), NCOA4, FTH (Cell signaling Technology, Danvers, MA, USA), and Transferrin Receptor (Thermo Fisher) antibodies. Anti-β-actin (BD Biosciences) antibodies were used as a loading control.

2.12. KRAS Mutation Profiling and Differential expressed gene analysis

Once the organoids were confirmed to be expanded after thawing, we performed whole exome sequencing, RNA- sequencing. The profiling of KRAS mutation was extracted from mutational profiles of whole-exome sequencing of PDPCOs provided by the Korean Cell Line Bank. Total DNA was isolated from the PDPCOs pellet using QIAamp DNA Mini Kit (Qiagen, Hilden, Germany) and the captured targets were subjected to sequencing using HiSeq 2500 (Illumina, San Diego, CA, USA). Total RNA was isolated from cell lysate using TRIzol (Qiagen, Hilden, Germany) and Qiagen RNeasy Kit (Qiagen, Hilden, Germany). Paired-end sequencing reads from cDNA libraries (101bp) were generated with an Illumina NovaSeq6000 instrument. The abundance of these transcripts in each sample was calculated as transcript per million mapped reads values and normalized with EdgeR.[33] Of the 62,000 Ensemble genes, we removed genes with minimal CPM values < 0.5. Differentially expressed genes (DEGs) analysis was performed with DESeq2 package using a threshold of false discovery rate < 0.1 and fold-change > 2.[34] Gene set enrichment analysis between ART responders and ART non-responders was performed using gene ontology as gene set database.[35] For pathway analysis, generally applicable gene set enrichment was used as a method, and Kyoto Encyclopedia of Genes and Genomes (KEGG) as gene sets.[36,37] For each of the significant KEGG pathways, the fold-changes of related genes on a pathway diagram using the Pathview Bioconductor package were used.[38] Also protein-protein interaction network analyses between results from DEGs and suspected key

mechanism of action of ART were conducted for further identification of core DEGs for the responsiveness of ART using the STRING database.[39] This database is freely available for use on the website: [http://string-db.org].

2.13. Statistical analysis

All data represent the mean ± standard error mean and were analyzed using a two-tailed Student's t-test. qPCR data are expressed as the mean ± standard deviation using a two-tailed Student's *t*-test. Statistical analyses and data processing were performed using Prism software 8 (GraphPad Inc.). A difference was considered statistically significant at the $P < 0.05$ level.

2.14. Ethics

This study was approved by the institutional review board of the Seoul National University Hospital, Korea (IRB No. H-2201-138-1294, IACUC No. 21-0249-S1A0), and all methods were carried out by relevant guidelines and regulations.

Chapter 3. Results

3.1. Anticancer effect of artesunate in various pancreatic cancer cell lines and patient-derived pancreatic cancer organoids

Four PC cell lines (BxPC-3, AsPC-1, Panc-1, MiaPaCa-2) were treated with ART to confirm the anticancer effect. Most 3D-cultured PC cell lines showed a good response to ART but the response was remarkably decreased in the BxPC-3 ($KRAS^{WT}$) cell line with uncheckable IC_{50} of ART. (Figure 1A) The anticancer effect of ART was also confirmed in various PDPCOs. (Figure 1C) SNU-4354-TO, which harbored $KRAS^{WT}$, showed the least sensitivity to ART than other PDPCOs with KRAS mutation.

3.2. Anticancer effect of artesunate in oxaliplatin-resistant patient-derived pancreatic cancer organoids

ART maintains its efficacy to induce cell death in the patient-derived 2D-cultural model (SNU-4340-T) and organoid model (SNU-4340-TO), but the cytotoxic effect of OXA was remarkably weakened in the organoid model in comparison with the 2D-cultural model. (Figure 2A, Figure 2B) Three PDPCOs (SNU-3947-TO, SNU-4206-TO, SNU-4340-TO) showed OXA-resistance (Figure 2C), and ART showed the effective cytotoxic effect on these OXA-resistant PDPCOs.

(Figure 2D)

3.3. Combinatorial effect of artesunate with oxaliplatin

The combinatorial anticancer effect of ART with OXA was evaluated in three PC cell lines with KRAS mutation. All PC cell lines showed sensitivity to ART and OXA, respectively. It was observed that more significant cell death occurred with a combination of ART and OXA. (Figure 3A) The synergy score was 33.78 in AsPC-1, 29.539 in MiaPaCa-2, and 21.189 in Panc-1. According to the synergy score, ART and OXA showed synergistic effects in all PC cell lines. ART and OXA showed effective inhibition of invasion and migration of 2D-cultured PC cell lines, and the combinatorial effect of ART and OXA were also observed. (Figure 3B, Figure 3C) ART showed better efficacy to inhibit sphere formation of PC cell lines than OXA, and a combination of both drugs showed significantly better efficacy. (Figure 3D, Figure 3E)

The effect of ART, OXA, and their combinatorial treatment was evaluated in 4 PDPCOs including one $KRAS^{WT}$ PDPCO (SNU-4354-TO), 3 KRAS-mutated PDPCOs (SNU-3947-TO, SNU-4305-TO, SNU-4340-TO). (Figure 4A, Figure 4B) ART did not show a significant effect in a $KRAS^{WT}$ PDPCO. In KRAS-mutated PDPCOs, there were differences in responsiveness to ART according to the subtype of KRAS mutation. PDPCOs with $KRAS^{G12D}$ (SNU-3947-TO and SNU-4305-TO) did not show a response to ART single treatment, but PDPCOs with $KRAS^{G12V}$ (SNU-4340-TO) showed a response to ART single treatment in comparison with the vehicle. PDPCOs showed more sensitivity to the combination of both drugs than each single drug. Combinatorial treatment of ART and OXA effectively induced cell

death even in these PDPCOs with OXA resistance. The synergy score was 6.849 in SNU-4354-TO (KRAS wild type), which means additive interaction. The synergy score was 10.511 in SNU-3947-TO, 13.316 in SNU-4305-TO, 10.718 in SNU-4340-TO, and 20.838 in SNU-4206-TO. ART and OXA showed synergistic effects in all PDPCOs that harbored KRAS mutation.

3.4. Anticancer effect of artesunate-induced ferroptosis

The cytotoxic effect of ART on 2D-cultured PC cell lines was blocked with the pretreatment of Fer-1, DFO, and Trolox. (Figure 5A) PC cell lines treated with ART showed elevated levels of C11-BODIPY fluorescence by lipid peroxidation, which was inhibited with Fer-1. (Figure 5B) Other methods for lipid peroxidation by measurement of malondialdehyde concentration and its reversal with ferroptosis inhibitors were confirmed. (Figure 5C) The elevated level of intracellular ROS was detected by DCF-DA fluorescence assay for ART-induced ferroptosis, which was inhibited with Fer-1. (Figure 5D) However, the apoptosis inhibitor (zVAD.fmk) did not inhibit the cytotoxic effects of ART for PC cell lines. (Figure 5E)

3.5. Role of ART-induced ferroptosis in combinatorial effect with OXA

PC cell lines treated with ART showed elevated MFI levels of C11-BODIPY fluorescence by lipid peroxidation, and it was enhanced with combinatorial treatment with OXA. (Figure 6A) ART increased the MFI level of Calcein-AM

fluorescence which was accompanied by the increased amount of intracellular labile iron pool (LIP). (Figure 6B) Increased ROS level, which was detected by DCF-DA fluorescence, was induced by ART and OXA of each single treatment, and combinatorial treatment showed a higher level of ROS. (Figure 6C) ART and OXA made mitochondrial damage with the increased levels of mitochondrial ROS, which was detected by MitoSOX fluorescence. (Figure 6D) ART induced a higher level of mitochondrial ROS than OXA, and combinatorial treatment lead to the significantly high level of mitochondrial ROS than each single treatment.

3.6. Key mechanism associated with artesunate-induced ferroptosis in pancreatic cancer

To explore the key mechanism of artesunate-induced ferroptosis in pancreatic cancer, the expression patterns of the four genes, which are cornerstones for ferroptosis, were identified in each cell line, and consistent overexpression patterns were found in the genes involved in iron hemostasis, and they were most upregulated in the combinatorial treatment. (Figure 7A) Protein level expression showed also consistent with the result of RNA expression pattern, and it seems the key pathway of ART-induced ferroptosis is dysregulation of iron metabolism and homeostasis, which were regulated with transferrin receptor, DMT1 (SLC11A2), NCOA4, and ferritin heavy chain. (Figure 7B) The overexpression level of RNA and level of protein associated with system Xc^- transporter (GPX4, SLC7A11, SLC3A2) is observed, which means increasing the intracellular reductive capacity, rather than killing cancer cells.

3.7. Result of differential expressed gene analysis and gene set enrichment analysis according to response for artesunate

To find a predictive factor of responders for ART, DEGs analysis was conducted for responders to ART (SNU-4206-TO, SNU-4340-TO) and non-responders to ART (SNU-4354-TO, SNU-3947-TO, SNU-4305-TO). A total of 148 genes were upregulated and 279 genes were downregulated in ART non-responders. (Figure 8A, 8B) The range of log2 fold change of DEGs was measured from -25.4291 to 26.60278. (Figure 8C) The top 50 genes were extracted by conducting gene enrichment analysis using KEGG genesets among total differential expressed gene sets between responders and non-responders to ART. In addition, functional protein association networks analysis with three iron homeostasis-related genes (TFRC, DMT1 (SLC11A2), FTH1), which were revealed as a key target proteins of ART-induced ferroptosis in PC in this study. Finally, the upregulation of ceruloplasmin (CP) was suspected to be a predictive factor for the non-responsiveness of ART. (Figure 8D) In addition, KEGG pathway analysis for ferroptosis showed CP act at an important step of iron homeostasis that converts Fe^{2+} to Fe^{3+} and promotes the binding of iron to transferrin. (Figure 8E) Based on the results, Figure 9 showed a schematic diagram of ART-induced ferroptosis, and role of .

Chapter 4. Discussion

ART showed a significant anticancer effect with ferroptosis to PC in this study, and its effect was maintained not only in 2D-cultural PC cell lines but also in PDPCOs. ART effectively induced cell death in PDPCOs that show resistance to OXA. Also, the synergistic effect of ART with OXA was shown with the enhanced level of ferroptosis. It is shown to respond more effectively to ART in the PDPCOs harbored $KRAS^{G12V}$ mutation, and ART showed a synergistic effect in PDPCOs with KRAS mutation regardless of the subtype. ART effectively induced ferroptosis in PC to induce the elevated level of intracellular iron level by overexpression of iron-import metabolic pathway including TFRC and DMT1 (SLC11A2). Upregulated expression of CP was suspected to be involved in inhibiting the effect of ART-induced dysregulation of iron homeostasis.

Ferroptosis is dependent upon intracellular iron, and its morphological, biochemical, and genetic features are distinct from apoptosis, necroptosis, and autophagy.[8] Ferroptosis is a result of metabolic dysfunction involving ROS accumulation, elevated level of intracellular iron, and peroxidation of polyunsaturated fatty acid, and the main regulatory pathways are modulation of their metabolism.[9] According to the findings of the current study, ART induces ferroptosis by upregulation of iron import with TFRC and DMT1 (SLC11A2), which result in the increased level of ferritin and activation of ferrinophagy to elevate levels of intracellular LIP and make PC cell prone to lipid peroxidation. In this aspect, ART was classified as a class IV ferroptosis inducer (FIN), which induces ferroptosis by direct iron overload or excessive activity of heme oxygenase 1. This finding is

consistent with the differential mRNA expression profile of genes involved in iron homeostasis in the previous study that suggested ART interactions with lysosomal iron to generate a sufficient level of ROS to overcome the capacity of the antioxidant response leading to lipid peroxidation and ferroptosis in PC cells.[20] In the current study, it was confirmed that these differential gene expression patterns leads to different phenotype. Meanwhile, the Xc^- system (SLC7A11 and SLC3A2) was overexpressed by ART treatment rather than directly inhibited in the current study, which can be interpreted as increasing their expression of them to compensate for the increased oxidative stress.

Interestingly, core differential expressed gene analysis between ART responder and ART non-responder identified the overexpression of CP is related to the resistance of ART. CP is a copper-containing glycoprotein that performs a major role in iron homeostasis by suppressing ferrous iron-mediated oxidative stress.[40] CP converts Fe^{2+} to Fe^{3+}_as ferroxidase and induces binding of iron to TFRC.[40,41] Recent study reported the inhibitory effect of CP for ferroptosis by regulating iron homeostasis in hepatocellular carcinoma cells.[42] CP assists ferroportin to export Fe^{2+} and suppresses ferroptosis and knockdown of CP promotes ferroptosis in hepatocellular cells by the accumulation of intracellular Fe^{2+}.[42] Also, elevated CP promoted HIF1α expression by reducing intracellular iron forming a positive feedback loop.[43] The expression and function of copper and copper metabolism MURR1 domain 10 suppress HIF1α / CP loop to enhance ferroptosis by disrupting copper-iron homeostasis.[43] Taken together with the results of the current study, it suggested that the expression level of CP can be an important biomarker in predicting the ferroptosis of PC.

Constitutive activation of KRAS drives many of the features of cancer, continuous proliferation, resistance to apoptosis, alteration of the tumor microenvironment, reconstruction of metabolism, immune evasion, cell migration, and metastasis.[44] According to the landscape of genomic alterations in PC, 93% of PC harbor KRAS mutation, and PC cells are highly resistant to apoptosis initiation and execution.[6,45] In the current study, ART showed a better effect in the 3D cultural PC cell lines and PDPCOs that harbor mutations in KRAS in comparison with KRAS wild-type cell lines and PDPCOs. This result was in line with the previous study, which reported the most effective ART-mediated death induction in PC cells expressing mutationally-active KRAS.[20] While PC cells are insensitive to apoptotic signaling, KRAS mutation may alter the metabolic environment of PC cells sensitized to ferroptosis.[20] This feature, prone to ferroptosis, was suggested to be induced by metabolic reprogramming by KRAS mutation lead up-regulation of transferrin receptor and down-regulation of ferritin.[8,10,46] This mechanism, KRAS-driven ferroaddiction, causes iron dependency that explains the induction of ferroptosis is less effective in KRAS wild-type PC cell lines and PDPCOs. However, the response to ART differs among KRAS mutation PDPCOs according to the subtype of KRAS mutation in the current study. PDPCOs with $KRAS^{G12V}$ showed effective cell death by ART, but $KRAS^{G12D}$ did not. In this context, $KRAS^{G12V}$ mutation seemed to be the most proper target for ART-induced anti-cancer treatment, but all PDPCOs that harbored KRAS mutation showed a synergistic effect of ART and OXA regardless of responsiveness to ART, while only additive effect was shown in KRAS wild type PDPCO. It seems that PC cells with KRAS mutation have a more important meaning from the perspective of overcoming the resistance of OXA. It has been reported that the PC with KRAS mutation has a worse prognosis than the PC

with KRAS wild type, and the $KRAS^{G12D}$ mutation has the worst prognosis among KRAS mutation subtypes.[47-50] The RAS protein is differentially coupled to downstream signaling pathways depending on the type of mutation.[51] The mutation subtype $KRAS^{G12D}$ is associated with phosphorylation and coupling of the PI3K/AKT and MEK pathway, while the mutation subtype $KRAS^{G12V}$ mainly activates the RAF/Ral pathway and induces de-phosphorylation of AKT.[49,51] The PC with $KRAS^{G12D}$ mutation was known to be more relevant with disease progression, metastatic features, and resistance to chemotherapeutic agents.[52,53] These aspects could be one of the possible explanations for the different responses to ART in the current study. It is better to conduct further research with a focus on subtypes of KRAS mutation in the future to find more proper indications for ART treatment.

OXA is a representative mainstay drug used in PC treatment, and it seems to be important to defeat resistance or non-responsiveness of PC for it. The current study suggested that ART might have an effect to overcome OXA resistance in PC, and the consistent results were confirmed in different PDPCOs. Overcoming the OXA resistance was explained with ART-induced ferroptosis, which was a completely different regulated cell death from apoptosis. But the synergistic effect of OXA and ART was not explained clearly with this explanation. Recently, intracellular conditions, which were prone to ferroptosis such as suppressing the KIF20A/NUAK1/Nrf2/GPX4 signaling pathway, restore or enhance sensitivity to oxaliplatin.[15,54] GPX4 is the main negative regulator of ferroptosis by reduction of lipid hydroperoxides, which was directly inhibited by class II or III FINs.[8,55,56] Nrf2 is a key regulator of anti-oxidant response including the expression of system Xc^-.[57-59] In addition, a recent study reported that OXA also kills tumor cells via oxidative stress by inhibiting the Nrf2 signaling pathway to induce ferroptosis.[60] The

synergistic effect of OXA and ART in the current study might be explained by the enhanced responsiveness of tumor cells to OXA by ART-induced oxidative stress enough to induce ferroptosis. Further study for validation of combinatorial treatment of ART and OXA in human subjects is needed. Like several clinical trials in other malignancies including breast cancer (ClinicalTrials.gov ID: NCT00764036), colorectal cancer (ClinicalTrials.gov ID: NCT02633098), hepatocellular carcinoma (ClinicalTrials.gov ID: NCT02304289), further clinical trial to evaluate the efficacy of ART for PC in combinatorial treatment and overcome chemo-resistance might be conducted in near future.

There were several strengths in this study. First, intensive efforts were made to confirm ferroptosis with various methods and materials. The definite marker of ferroptosis is not determined, so it seemed to be important to check the consistent experimental results from various stages of metabolic pathways, such as Lipid peroxidation, ROS production, mitochondrial ROS production, and LIP assay. In addition, three ferroptosis inhibitors, Fer-1, Trolox, and DFO, which suppress different steps of ferroptosis, were used in current study and consistent results could be confirmed.[8,20,61] Second, a large number of PDPCOs were used in the current study to verify the effect of ART-induced ferroptosis. Scaffold-based models, such as PDPCOs, reflects features modulation of the response to chemotherapy, immunotherapy, and radiation, and more readily mimic cell-to-extracellular matrix interactions.[22,62] Since consistent results were confirmed in various PDPCOs in ART-induced ferroptosis, overcoming OXA resistance, and synergistic effect with OXA, ART seems to be a promising drug for PC treatment. Third, possible biomarkers were suggested in this study that may possibly distinguish responders for ART. Although additional verifications are needed in further studies, considering that the effect of

ART may decrease in the case of having $KRAS^{G12D}$ mutation or overexpression of CP, these can be applied as a biomarker to reasonably find better individuals in future clinical trials and precision medicine.

There were several limitations in this study. First, it is difficult to completely explain the synergistic effect of OXA and ART. The efforts for the underlying mechanism of this synergistic effect were performed in the current study, and further induction of ferroptosis was found, but further explanation with a more sophisticated study of molecular biological mechanisms is needed. In addition, it is necessary to evaluate whether combination therapy with other chemotherapeutic agents or drug resistance can be overcome with ART. Second, validation experiments with xenograft models were not conducted. Considering the desmoplastic tumor microenvironment and the action of the immune system of PC, it seems that in vivo validation using the xenograft model cannot be completely replaced by cancer organoids yet. Still, all PDPCOs, which were used in the current study, were established using core biopsy tissues directly collected from patients in our institution and harbor different features and environments. These might partly make up for the shortcomings of in vitro models in the current study.

Chapter 5. Conclusions

ART showed promising anticancer effects by ferroptosis for PC. The mechanism of ART-induced ferroptosis is changing iron metabolism and iron homeostasis. Effective cell death was observed in PC cell lines with KRAS mutation and PDPCOs with KRAS mutation. PDPCOs with $KRAS^{G12V}$ mutation subtype showed the most effective cell death by ART. Effective cell death was also maintained even in the OXA-resistant PDPCOs, and the synergistic anticancer effect was confirmed by combinatorial treatment of OXA and ART. Upregulation of CP level was suspected to be a biomarker for the prediction of responsiveness for ART. Clinical trials in human subjects with proper features to overcome OXA resistance in PC using ART are needed in near future.

Tables

Table 1. List of pancreatic cancer cell lines and patients-derived pancreatic cancer organoids used in the study

Type	Name	KRAS	Feature
Cell line	BxPC-3	Wild type	Classical type
Cell line	Panc-1	Mutation (G12D)	Quasi-mesenchymal type
Cell line	AsPc-1	Mutation (G12D)	Classical type
Cell line	MiaPaCa-2	Mutation (G12C)	Quasi-mesenchymal type
Cell line	SNU-4340-T	Mutation (G12V)	OXA resistant
PDPCO	SNU-4354-TO	Wild type	OXA resistant
PDPCO	SNU-3947-TO	Mutation (G12D)	OXA resistant
PDPCO	SNU-4206-TO	Mutation (G12V)	OXA resistant
PDPCO	SNU-4305-TO	Mutation (G12D)	OXA resistant
PDPCO	SNU-4340-TO	Mutation (G12V)	OXA resistant

Figures

Figure 1. Anticancer effect of artesunate in various pancreatic cancer. (A) Cytotoxic effect of artesunate in 3D culture model after 48 hours (B) Cytotoxic effect of artesunate in patients-derived pancreatic cancer organoids after 48 hours

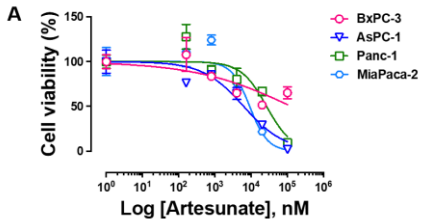

Cell line	BxPC-3	AsPC-1	Panc-1	MiaPaca-2
KRAS	Wild type	G12D	G12D	G12C
IC_{50} (μM)	>100	6.2	26.7	9.1

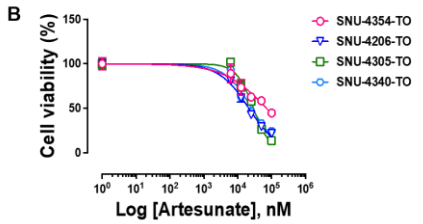

PDPCOs	SNU-4354-TO	SNU-4206-TO	SNU-4305-TO	SNU-4340-TO
KRAS	Wild type	G12V	G12D	G12V
IC_{50} (μM)	71.0	21.3	29.0	26.1

Figure 2. Anticancer effect of artesunate in oxaliplatin resistant patients-derived pancreatic cancer organoids. (A) Cytotoxic effect of artesunate in 2D culture model and organoid model (B) Cytotoxic effect of oxaliplatin in 2D culture model and organoid model (C) Cytotoxic effect of artesunate in patients-derived pancreatic cancer organoids model (D) Cytotoxic effect of oxaliplatin in patients-derived pancreatic cancer organoids model

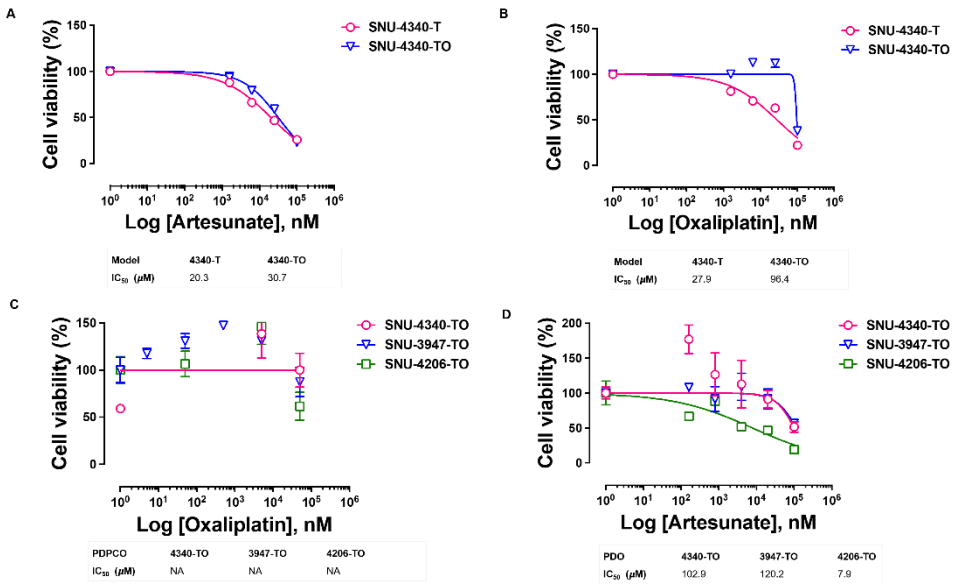

Figure 3. Combinatorial effect of artesunate with oxaliplatin in pancreatic cancer cell lines. (A) Cell viability test in pancreatic cancer cell lines (B, C) Migration and invasion assay in pancreatic cancer cell lines (D, E) Sphere formation ability test with pancreatic cancer cell lines

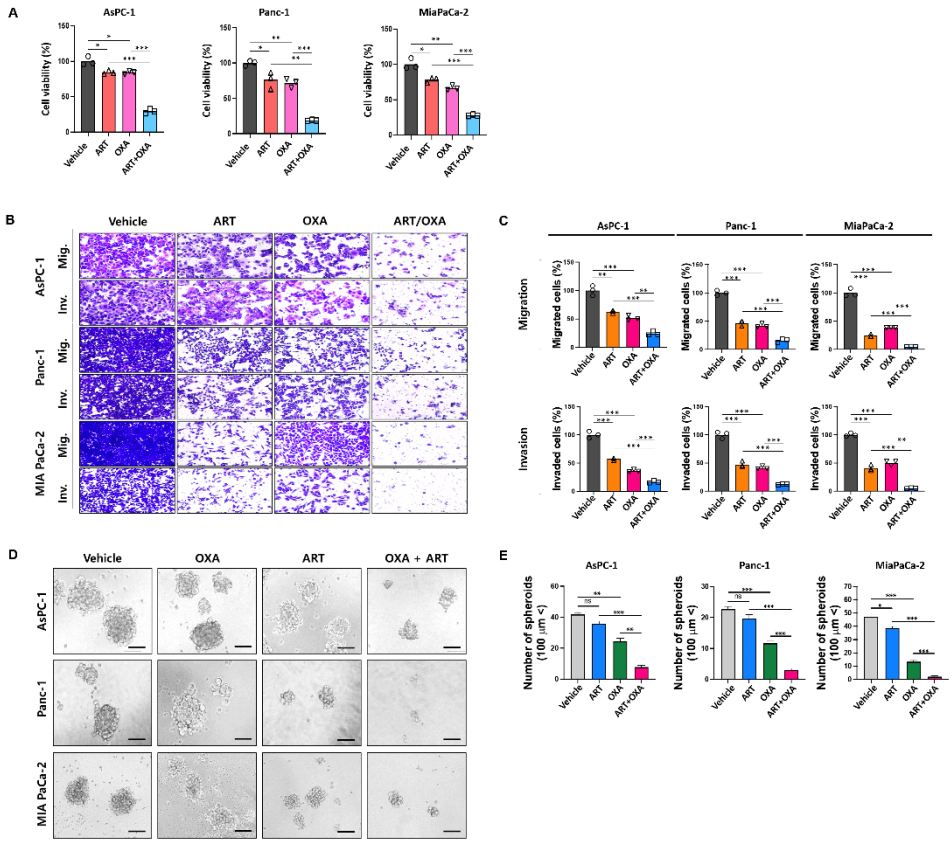

Figure 4. Result of artesunate, oxaliplatin, and their combinatorial treatment for patients-derived pancreatic cancer organoids. (A) Result of cell viability assay for artesunate, oxaliplatin, and their combinatorial treatment for eight patients-derived pancreatic cancer organoids (B) Representative confocal images of patients-derived pancreatic cancer organoids

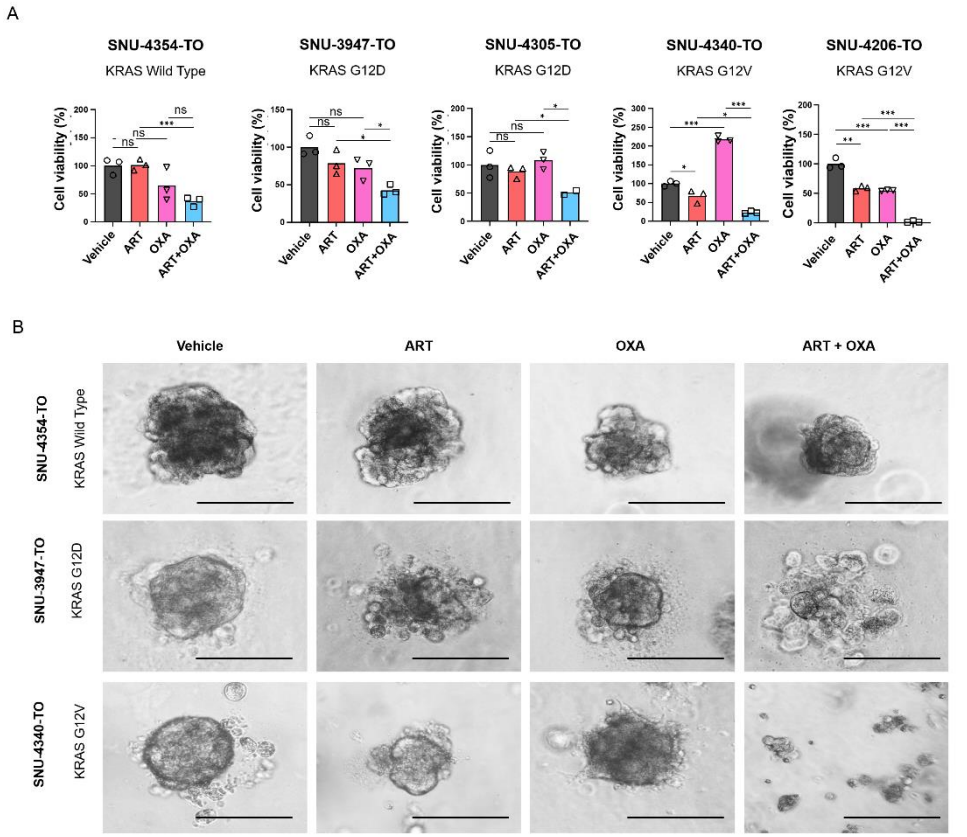

Figure 5. Artesunate-induced ferroptosis is a key mechanism of anticancer effect for pancreatic cancer. (A) cytotoxic effect of ART and reversal with ferroptosis inhibitors (B) Lipid peroxidation with C11-BODIPY fluorescence assay for ART-induced lipid peroxidation and its reversal with Fer-1 (C) Lipid peroxidation assay with measurement of malondialdehyde concentration and its reversal with ferroptosis inhibitors (D) DCF-DA fluorescence assay for ART-induced ferroptosis and its reversal with Fer-1 (E) Cytotoxic effect of ART and no reverse effect with an apoptosis inhibitor

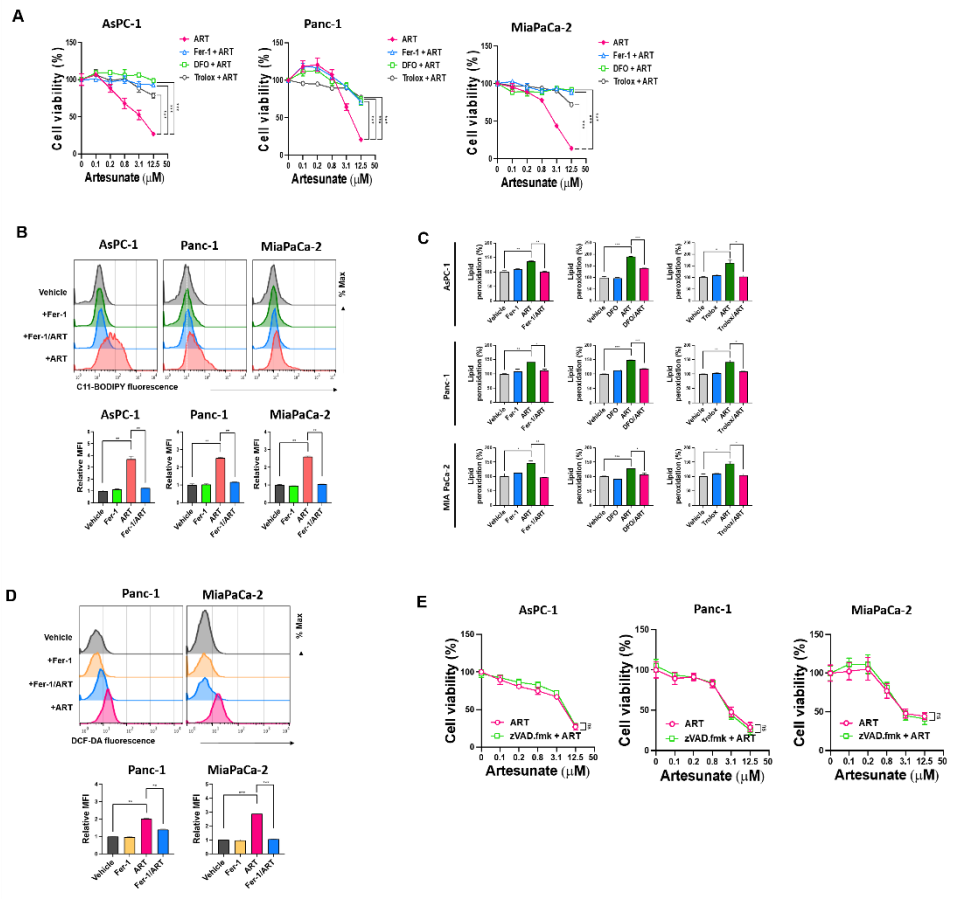

Figure 6. Role of ferroptosis in the combinatorial effect of artesunate and oxaliplatin. (A) Result of lipid peroxidation assay (B) Result of labile iron pool assay (C) Result of detection of ROS level (D) Result of mitochondrial ROS assay

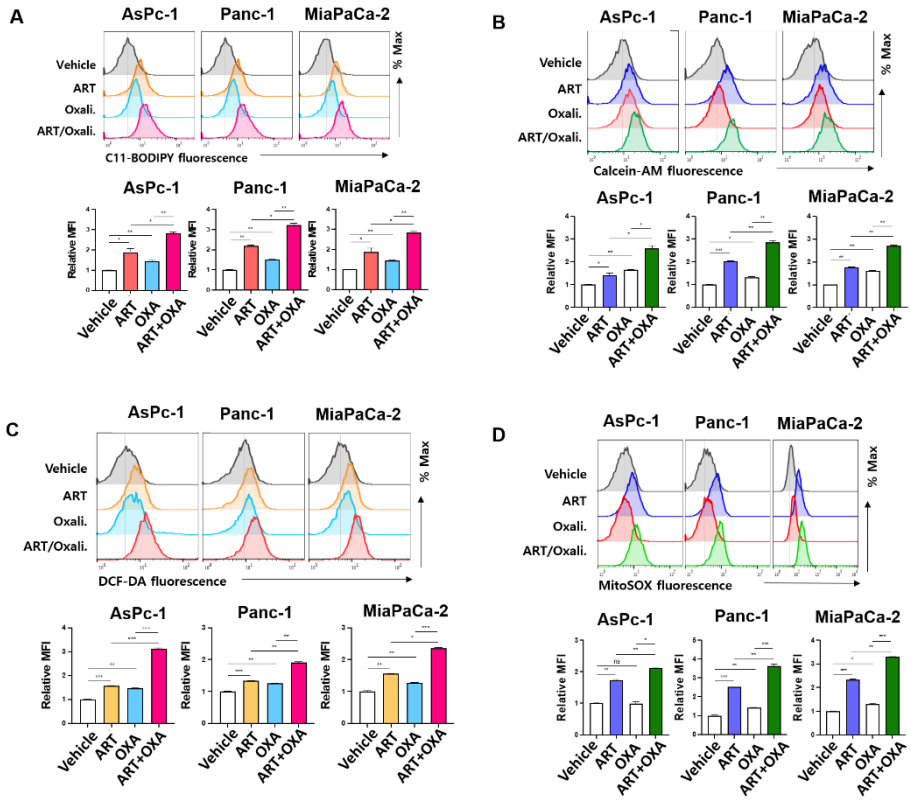

Figure 7. Exploration of artesunate-induced ferroptosis. (A) Result of iron metabolism-related RNA expression (B) Result of a western blot for iron metabolism pathway

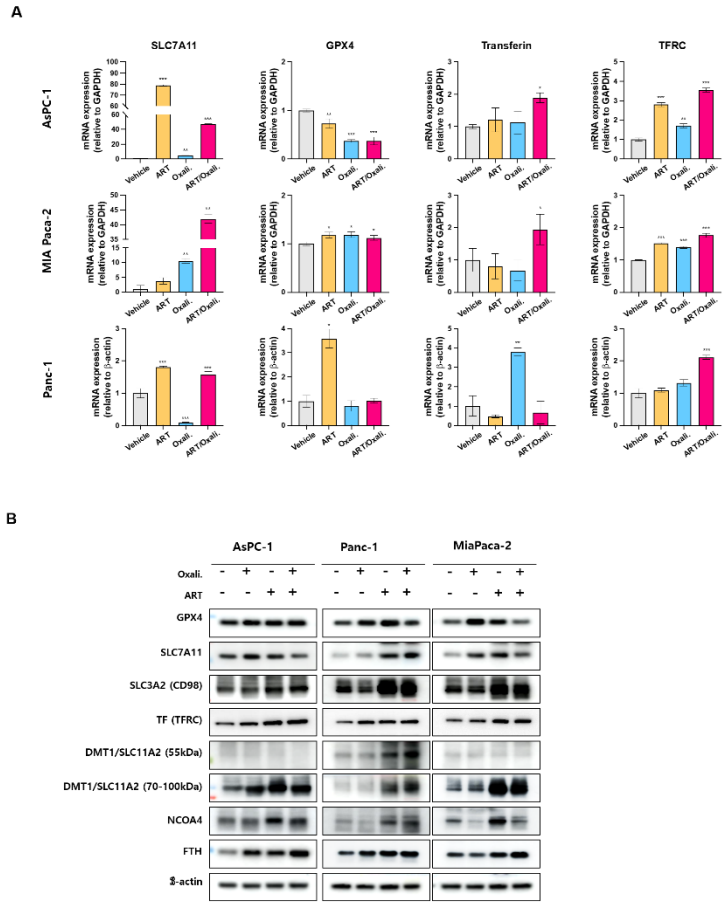

Figure 8. Result of differential expressed gene analysis and gene set enrichment analysis according to response for artesunate. (A) The number of differentially expressed genes between ART responder and ART non-responder (B) Heatmap of differentially expressed genes between ART responder and ART non-responder (C) Volcano plot of differentially expressed genes between ART responder and ART non-responder (D) Identification of core differentially expressed genes between responders and non-responders. Consideration of top 50 genes from the comparison of enrichment analysis by KEGG pathway and functional protein association networks analysis with iron homeostasis related genes by Sting-DB. The bottom panel shows the result of identified genetic alterations in the non-responders. (E) Ferroptosis-related pathway analysis with KEGG database

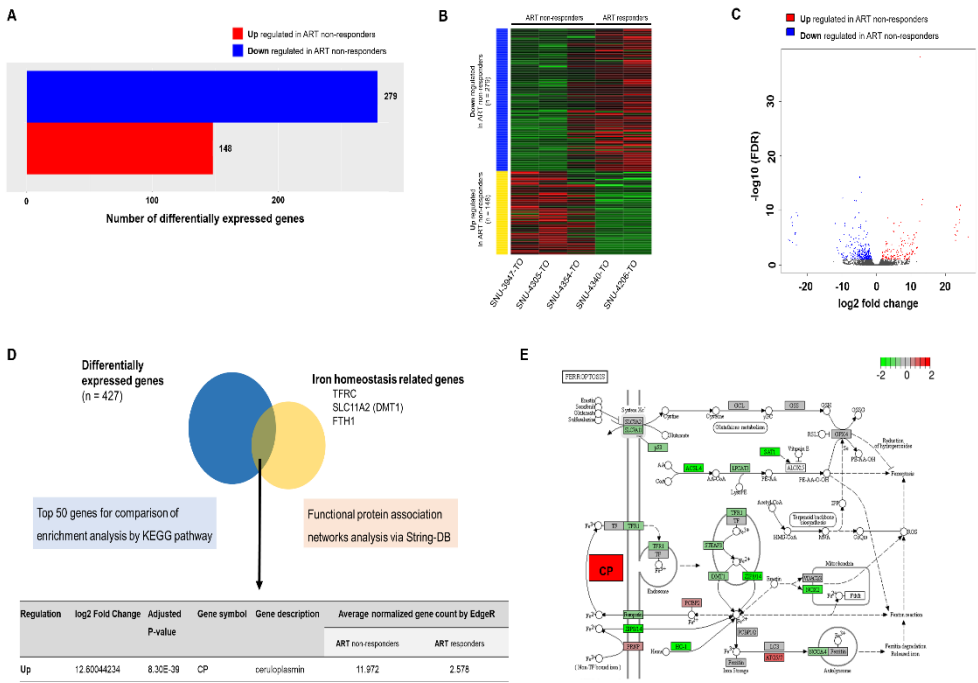

Regulation	log2 Fold Change	Adjusted P-value	Gene symbol	Gene description	Average normalized gene count by EdgeR	
					ART non-responders	ART responders
Up	12.60044234	8.30E-39	CP	ceruloplasmin	11.972	2.578

Figure 9. The schematic diagram for the mechanism of artesunate-induced ferroptosis

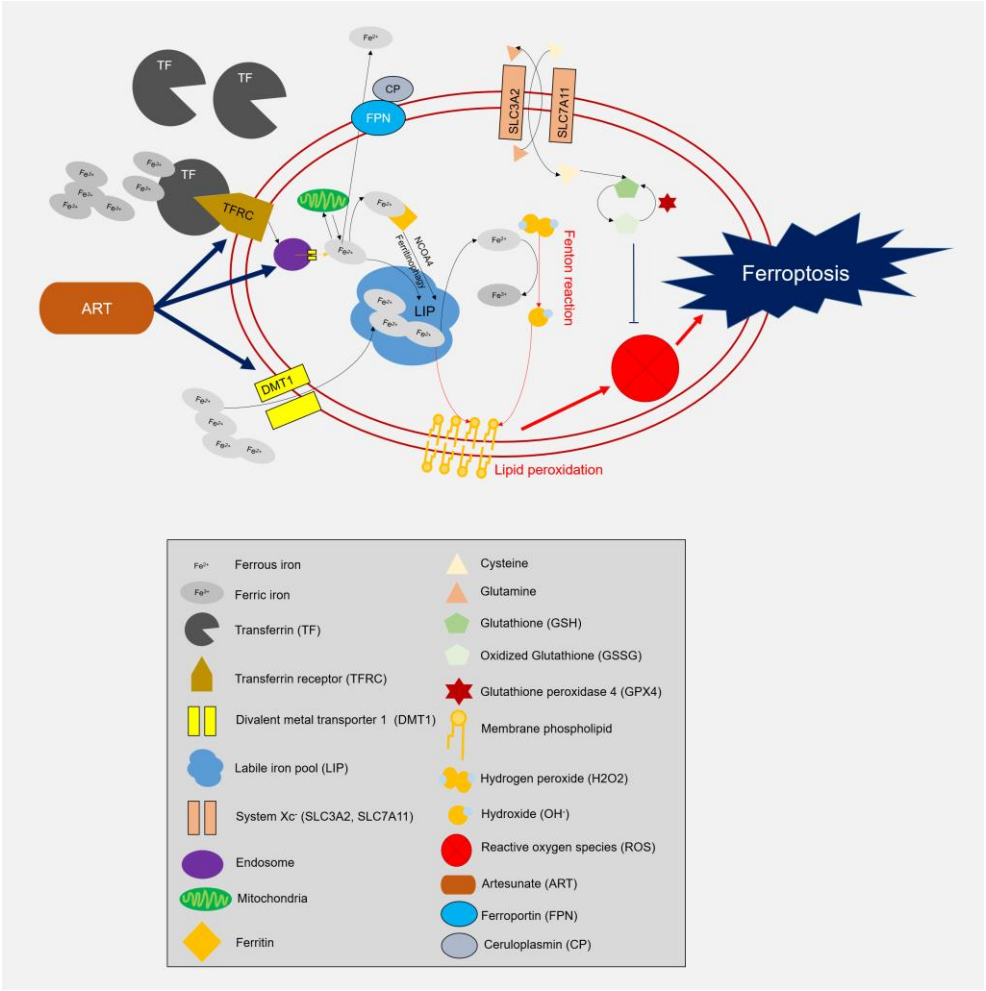

References

1. Rahib L, Smith BD, Aizenberg R, Rosenzweig AB, Fleshman JM, Matrisian LM. Projecting cancer incidence and deaths to 2030: the unexpected burden of thyroid, liver, and pancreas cancers in the United States. Cancer research 2014;74:2913-21.

2. Kamisawa T, Wood LD, Itoi T, Takaori K. Pancreatic cancer. Lancet (London, England) 2016;388:73-85.

3. Conroy T, Desseigne F, Ychou M, et al. FOLFIRINOX versus gemcitabine for metastatic pancreatic cancer. The New England journal of medicine 2011;364:1817-25.

4. Von Hoff DD, Ervin T, Arena FP, et al. Increased survival in pancreatic cancer with nab-paclitaxel plus gemcitabine. The New England journal of medicine 2013;369:1691-703.

5. Buscail L, Bournet B, Cordelier P. Role of oncogenic KRAS in the diagnosis, prognosis and treatment of pancreatic cancer. Nature reviews Gastroenterology & hepatology 2020;17:153-68.

6. Network CGAR. Integrated Genomic Characterization of Pancreatic Ductal Adenocarcinoma. Cancer cell 2017;32:185-203.e13.

7. Santofimia-Castaño P, Iovanna J. Combating pancreatic cancer chemoresistance by triggering multiple cell death pathways. Pancreatology : official journal of the International Association of Pancreatology (IAP) [et al] 2021;21:522-9.

8. Dixon SJ, Lemberg KM, Lamprecht MR, et al. Ferroptosis: an iron-dependent form of nonapoptotic cell death. Cell 2012;149:1060-72.

9. Hassannia B, Vandenabeele P, Vanden Berghe T. Targeting Ferroptosis to Iron Out Cancer. Cancer cell 2019;35:830-49.

10. Andreani C, Bartolacci C, Scaglioni PP. Ferroptosis: A Specific Vulnerability of RAS-Driven Cancers? Frontiers in oncology 2022;12:923915.

11. Markowitsch SD, Schupp P, Lauckner J, et al. Artesunate Inhibits Growth of Sunitinib-Resistant Renal Cell Carcinoma Cells through Cell Cycle Arrest and Induction of Ferroptosis. Cancers 2020;12.

12. Sun Y, Qiao Y, Liu Y, et al. ent-Kaurane diterpenoids induce apoptosis and ferroptosis through targeting redox resetting to overcome cisplatin resistance. Redox biology 2021;43:101977.

13. Roh JL, Kim EH, Jang HJ, Park JY, Shin D. Induction of ferroptotic cell death for overcoming cisplatin resistance of head and neck cancer. Cancer letters 2016;381:96-103.

14. Turcu AL, Versini A, Khene N, et al. DMT1 Inhibitors Kill Cancer Stem Cells by Blocking Lysosomal Iron Translocation. Chemistry (Weinheim an der Bergstrasse, Germany) 2020;26:7369-73.

15. Yang C, Zhang Y, Lin S, Liu Y, Li W. Suppressing the KIF20A/NUAK1/Nrf2/GPX4 signaling pathway induces ferroptosis and enhances the sensitivity of colorectal cancer to oxaliplatin. Aging 2021;13:13515-34.

16. Chen TC, Chuang JY, Ko CY, et al. AR ubiquitination induced by the curcumin analog suppresses growth of temozolomide-resistant glioblastoma through disrupting GPX4-Mediated redox homeostasis. Redox biology 2020;30:101413.

17. Fu D, Wang C, Yu L, Yu R. Induction of ferroptosis by ATF3 elevation alleviates cisplatin resistance in gastric cancer by restraining Nrf2/Keap1/xCT signaling. Cellular & molecular biology letters 2021;26:26.

18. Yang WS, Stockwell BR. Ferroptosis: Death by Lipid Peroxidation. Trends in cell biology 2016;26:165-76.

19. Ye J, Zhang R, Wu F, et al. Non-apoptotic cell death in malignant tumor cells and natural compounds. Cancer letters 2018;420:210-27.

20. Eling N, Reuter L, Hazin J, Hamacher-Brady A, Brady NR. Identification of artesunate as a specific activator of ferroptosis in pancreatic cancer cells. Oncoscience 2015;2:517-32.

21. Lee JH, Kim H, Lee SH, et al. Establishment of Patient-Derived Pancreatic Cancer Organoids from Endoscopic Ultrasound-Guided Fine-Needle Aspiration Biopsies. Gut and liver 2022;16:625-36.

22. Langhans SA. Three-Dimensional in Vitro Cell Culture Models in Drug Discovery and Drug Repositioning. Frontiers in pharmacology 2018;9:6.

23. Kim J, Koo BK, Knoblich JA. Human organoids: model systems for human biology and medicine. Nature reviews Molecular cell biology 2020;21:571-84.

24. Sugimoto S, Sato T. Organoid vs In Vivo Mouse Model: Which is

Better Research Tool to Understand the Biologic Mechanisms of Intestinal Epithelium? Cellular and molecular gastroenterology and hepatology 2022;13:195-7.

25. Mittler F, Obeïd P, Rulina AV, Haguet V, Gidrol X, Balakirev MY. High-Content Monitoring of Drug Effects in a 3D Spheroid Model. Frontiers in oncology 2017;7:293.

26. Pijuan J, Barceló C, Moreno DF, et al. In vitro Cell Migration, Invasion, and Adhesion Assays: From Cell Imaging to Data Analysis. Frontiers in cell and developmental biology 2019;7:107.

27. Longati P, Jia X, Eimer J, et al. 3D pancreatic carcinoma spheroids induce a matrix-rich, chemoresistant phenotype offering a better model for drug testing. BMC cancer 2013;13:95.

28. DeHart DN, Fang D, Heslop K, Li L, Lemasters JJ, Maldonado EN. Opening of voltage dependent anion channels promotes reactive oxygen species generation, mitochondrial dysfunction and cell death in cancer cells. Biochemical pharmacology 2018;148:155-62.

29. Kauffman ME, Kauffman MK, Traore K, et al. MitoSOX-Based Flow Cytometry for Detecting Mitochondrial ROS. Reactive oxygen species (Apex, NC) 2016;2:361-70.

30. Wiernicki B, Dubois H, Tyurina YY, et al. Excessive phospholipid peroxidation distinguishes ferroptosis from other cell death modes including pyroptosis. Cell death & disease 2020;11:922.

31. Miotto G, Rossetto M, Di Paolo ML, et al. Insight into the mechanism

of ferroptosis inhibition by ferrostatin-1. Redox biology 2020;28:101328.

32. Ianevski A, Giri AK, Aittokallio T. SynergyFinder 2.0: visual analytics of multi-drug combination synergies. Nucleic acids research 2020;48:W488-w93.

33. Robinson MD, Oshlack A. A scaling normalization method for differential expression analysis of RNA-seq data. Genome biology 2010;11:R25.

34. Love MI, Huber W, Anders S. Moderated estimation of fold change and dispersion for RNA-seq data with DESeq2. Genome biology 2014;15:550.

35. Schug TT, Nadadur SS, Johnson AF. Nano GO Consortium--a team science approach to assess engineered nanomaterials: reliable assays and methods. Environmental health perspectives 2013;121:A176-7.

36. Luo W, Friedman MS, Shedden K, Hankenson KD, Woolf PJ. GAGE: generally applicable gene set enrichment for pathway analysis. BMC bioinformatics 2009;10:161.

37. Kanehisa M, Sato Y, Kawashima M, Furumichi M, Tanabe M. KEGG as a reference resource for gene and protein annotation. Nucleic acids research 2016;44:D457-62.

38. Luo W, Brouwer C. Pathview: an R/Bioconductor package for pathway-based data integration and visualization. Bioinformatics (Oxford, England) 2013;29:1830-1.

39. Szklarczyk D, Franceschini A, Wyder S, et al. STRING v10: protein-protein interaction networks, integrated over the tree of life. Nucleic acids

research 2015;43:D447-52.

40. Bakhautdin B, Goksoy Bakhautdin E, Fox PL. Ceruloplasmin has two nearly identical sites that bind myeloperoxidase. Biochemical and biophysical research communications 2014;453:722-7.

41. Cherukuri S, Tripoulas NA, Nurko S, Fox PL. Anemia and impaired stress-induced erythropoiesis in aceruloplasminemic mice. Blood cells, molecules & diseases 2004;33:346-55.

42. Shang Y, Luo M, Yao F, Wang S, Yuan Z, Yang Y. Ceruloplasmin suppresses ferroptosis by regulating iron homeostasis in hepatocellular carcinoma cells. Cellular signalling 2020;72:109633.

43. Yang M, Wu X, Hu J, et al. COMMD10 inhibits HIF1α/CP loop to enhance ferroptosis and radiosensitivity by disrupting Cu-Fe balance in hepatocellular carcinoma. Journal of hepatology 2022;76:1138-50.

44. Pylayeva-Gupta Y, Grabocka E, Bar-Sagi D. RAS oncogenes: weaving a tumorigenic web. Nature reviews Cancer 2011;11:761-74.

45. Eser S, Schnieke A, Schneider G, Saur D. Oncogenic KRAS signalling in pancreatic cancer. British journal of cancer 2014;111:817-22.

46. Jiang H, Muir RK, Gonciarz RL, et al. Ferrous iron-activatable drug conjugate achieves potent MAPK blockade in KRAS-driven tumors. The Journal of experimental medicine 2022;219.

47. Qian ZR, Rubinson DA, Nowak JA, et al. Association of Alterations in Main Driver Genes With Outcomes of Patients With Resected Pancreatic Ductal Adenocarcinoma. JAMA oncology 2018;4:e173420.

48. Philip PA, Azar I, Xiu J, et al. Molecular Characterization of KRAS Wild-type Tumors in Patients with Pancreatic Adenocarcinoma. Clinical cancer research : an official journal of the American Association for Cancer Research 2022;28:2704-14.

49. Bournet B, Muscari F, Buscail C, et al. KRAS G12D Mutation Subtype Is A Prognostic Factor for Advanced Pancreatic Adenocarcinoma. Clinical and translational gastroenterology 2016;7:e157.

50. Ogura T, Yamao K, Hara K, et al. Prognostic value of K-ras mutation status and subtypes in endoscopic ultrasound-guided fine-needle aspiration specimens from patients with unresectable pancreatic cancer. Journal of gastroenterology 2013;48:640-6.

51. Ihle NT, Byers LA, Kim ES, et al. Effect of KRAS oncogene substitutions on protein behavior: implications for signaling and clinical outcome. Journal of the National Cancer Institute 2012;104:228-39.

52. Sun C, Rosendahl AH, Andersson R, Wu D, Wang X. The role of phosphatidylinositol 3-kinase signaling pathways in pancreatic cancer. Pancreatology : official journal of the International Association of Pancreatology (IAP) [et al] 2011;11:252-60.

53. Neuzillet C, Hammel P, Tijeras-Raballand A, Couvelard A, Raymond E. Targeting the Ras-ERK pathway in pancreatic adenocarcinoma. Cancer metastasis reviews 2013;32:147-62.

54. Wu F, Du Y, Yang J, et al. Peroxidase-like Active Nanomedicine with Dual Glutathione Depletion Property to Restore Oxaliplatin Chemosensitivity

and Promote Programmed Cell Death. ACS nano 2022;16:3647-63.

55. Yang WS, SriRamaratnam R, Welsch ME, et al. Regulation of ferroptotic cancer cell death by GPX4. Cell 2014;156:317-31.

56. Yang WS, Stockwell BR. Synthetic lethal screening identifies compounds activating iron-dependent, nonapoptotic cell death in oncogenic-RAS-harboring cancer cells. Chemistry & biology 2008;15:234-45.

57. Roh JL, Kim EH, Jang H, Shin D. Nrf2 inhibition reverses the resistance of cisplatin-resistant head and neck cancer cells to artesunate-induced ferroptosis. Redox biology 2017;11:254-62.

58. Sun X, Ou Z, Chen R, et al. Activation of the p62-Keap1-NRF2 pathway protects against ferroptosis in hepatocellular carcinoma cells. Hepatology (Baltimore, Md) 2016;63:173-84.

59. Fan Z, Wirth AK, Chen D, et al. Nrf2-Keap1 pathway promotes cell proliferation and diminishes ferroptosis. Oncogenesis 2017;6:e371.

60. Liu B, Wang H. Oxaliplatin induces ferroptosis and oxidative stress in HT29 colorectal cancer cells by inhibiting the Nrf2 signaling pathway. Experimental and therapeutic medicine 2022;23:394.

61. Subburayan K, Thayyullathil F, Pallichankandy S, Cheratta AR, Galadari S. Superoxide-mediated ferroptosis in human cancer cells induced by sodium selenite. Translational oncology 2020;13:100843.

62. Karlsson H, Fryknäs M, Larsson R, Nygren P. Loss of cancer drug activity in colon cancer HCT-116 cells during spheroid formation in a new 3-D spheroid cell culture system. Experimental cell research 2012;318:1577-85.

국문 초록

췌장암은 가장 예후가 좋지 않은 암 중에 하나이다. 췌장암 환자에 대한 세포독성 화학요법의 조합으로 기대수명이 연장되었음에도 불구하고, 약제의 저항성과 치료에 대한 저항성이 문제가 된다. 이러한 문제를 극복하고자 하는 것은 췌장암의 치료에 있어서 중요한 미충족 수요이며, 본 연구를 통해 췌장암의 세포주 및 환자 유래 췌장암 오가노이드를 이용하여 아르테수네이트 (artesunate) 유도 퍼롭토시스 (ferroptosis) 가 췌장암의 사멸에 미치는 영향을 평가하고자 한다. 본 연구에서는 잘 알려진 췌장암 세포주 4개와 KRAS 유전자의 야생형 및 변이형 유전자를 다양하게 포함하고, 옥살리플라틴 (oxaliplain) 저항성을 보이는 다양한 환자 유래 췌장암 오가노이드 5개를 사용하였다. 췌장암에 대한 아르테수네이트의 효능을 측정하기 위해서 세포 생존 분석 (Cell viability assay), 전이 및 침윤 분석 (migration and invasion assay), 구 형성 분석 (spheres formation assay) 을 수행하였다. 결과적으로 KRAS 유전자의 돌연변이가 있는 경우에 아르테수네이트에 대한 세포사멸 반응이 좋았으며, 특히 $KRAS^{G12V}$ 돌연변이를 가지는 경우 효과가 뛰어났다. 아르테수네이트는 옥살리플라틴과 병합할 경우 KRAS 돌연변이의 아형과는 관계없이 시너지효과 (synergistic effect) 를 보이는 것이 확인되었다. 반응성 산소종 검출 (Reactive oxygen species detection), 지질 과산화 분석 (lipid peroxidation assay), 불안정한 철 저장소 분석

(labile iron pool assay) 을 실시하여 퍼롭토시스를 통한 세포사멸에 대해 평가하였다. 아르테수네이트 유도 퍼롭토시스의 작용 기전을 확인하기 위해 정량적 실시간 PCR (real-time quantitative polymerase chain reaction) 과 웨스턴 블랏 (western blot) 을 통해 탐색하였다. 아르테수네이트는 세포자멸사 (apoptosis) 가 아닌 퍼롭토시스를 통해 췌장암 세포주 및 환자 유래 췌장암 오가노이드에 대해서 유의미한 세포사멸 효과를 보였다. 아르테수네이트는 옥살리플라틴에 저항성을 보이는 환자 유래 췌장암 오가노이드에서도 효과적으로 퍼롭토시스를 통한 세포사멸을 유도하였으며, 아르테수네이트와 옥살리플라틴의 병합치료는 시너지 효과가 나타남을 확인할 수 있었다. 아르테수네이트는 철분 대사 경로 유전자와 단백질의 과발현에 의해 세포 내 철분 수준 상승을 유도하고, 이 기전을 통해 췌장암에서 퍼롭토시스를 효과적으로 유도함을 확인했다. 본 연구를 통해 아르테수네이트에 의해 유발되는 퍼롭토시스가 췌장암에서 효과적이며, 옥살리플라틴의 저항성을 극복할 수 있는 유망한 암세포사멸효과를 가지는 것을 확인할 수 있었다. 아르테수네이트의 반응을 예측할 수 있는 유의유전자를 확인하기 위해 차등유전자발현 분석 (differentially expressed gene analysis), 유전자 집합 농축 분석 (gene set enrichment analysis), 기전 분석 (pathway analysis) 및 단백질간 상호작용 네트워크분석 (protein-protein interaction network analysis) 를 종합적으로 고려한 결과, 세룰로플라스민 (ceruloplasmin) 을 과발현하는 것이 아르테수네이트에 대한 좋지 않은 반응을 예측하는 바이오마커로서 활용할 수 있으리라 보여진다. 향후 아르테수네이트를

이용해 효과적으로 췌장암에서 치료효과에 대한 인간 대상 임상시험이 필요하다.

주요어 : 췌장암; 아르테수네이트; 퍼룹토시스; 오가노이드; 약제 저항성

학번 : 2020-30048